Curr Cardiovasc Imaging Rep (2014) 7:9289
DOI 10.1007/s12410-014-9289-6

Dual Energy Imaging in Cardiovascular CT: Current Status and Impact on Radiation, Contrast and Accuracy

Prabhakar Rajiah · Sandra S. Halliburton

Published online: 10 August 2014

Abstract Dual-energy computed tomography (DECT) exploits the continuous energy distribution of x-rays to improve differentiation of tissues beyond what is possible with single-energy CT (SECT). DECT often uses smaller volumes of iodinated contrast agent and lower radiation doses than SECT. Clinical applications of DECT in cardiovascular imaging are emerging and include myocardial perfusion imaging, myocardial infarct and viability imaging, coronary plaque characterization, coronary stent assessment, and myocardial iron quantification. In this review, we discuss the available methods for acquiring and processing DECT data, the current status of DECT in cardiovascular imaging, and its impact on the dose of radiation and contrast agent.

Keywords Cardiac · CT · Dual energy · Radiation dose · Contrast agent dose

Introduction

The principles of dual-energy computed tomography (DECT) are well known, but this technique has only recently been used for cardiovascular imaging. Diagnostic x-ray spectrums have a continuous energy distribution, with the highest energy determined by the peak tube potential. The dominant mechanisms of an x-ray photon's interaction with tissue vary with the energy of the photon, resulting in energy-dependent tissue attenuation. Higher-energy photons predominantly interact with tissue via Compton scattering, which is governed by tissue density. Lower-energy photons predominantly interact with tissue via the photoelectric effect; this interaction is largely governed by tissue atomic number. Differences in x-ray attenuation at higher versus lower energies are greatest in denser tissues; for example, iodine and calcium show large differences in dense tissues but the differences in soft tissue are minimal. In traditional single-energy CT (SECT), a single polychromatic x-ray beam interacts with tissues and the attenuated x-rays are integrated by solid-state detectors, preventing spectral differentiation of data. With DECT, two spectrally distinct datasets are obtained from the same region of interest, enabling differentiation of tissues based on atomic number and physical density [1].

In this review, we discuss available methods for acquiring and processing DECT data, the accuracy of DECT for specific cardiovascular applications, and the impact of DECT on the dose of radiation and contrast agent.

Acquisition of DECT Data

Four different technologies are currently available for DECT. Dual-source CT systems (Siemens Healthcare, Erlangen, Germany) are the most established. These systems use two x-ray tubes and two detector arrays mounted about 90° apart on the same gantry to simultaneously acquire two sets of attenuation data [2]. The tubes are operated at different peak tube potentials: one at 80 or 100 kVp, the other at 140 kVp. Two spectrally distinct datasets can also be acquired using a single-source system (GE Healthcare, Waukesha, WI) that quickly (0.2 ms) alternates the peak tube potential from 80 to 140 kVp for

This a article is part of the Topical Collection on *Cardiac Computed Tomography*

P. Rajiah (✉)
Cardiothoracic Imaging, Department of Radiology, University Hospital Cleveland Case Medical Center, Case Western Reserve University School of Medicine, 11100 Euclid Avenue, Cleveland, OH 44106, USA
e-mail: radprabhakar@gmail.com

S. S. Halliburton
Imaging Institute, Heart and Vascular Institute Cleveland Clinic, Cleveland, OH, USA

successive x-ray projections [3]. Dual-energy data can also be acquired with a single tube operating at a fixed tube potential and using two layers of detectors to record spectrally distinct data (Philips, Cleveland, OH) [4]. The upper and lower detector rows acquire attenuation data from low-energy and high-energy photons, respectively, with photons of higher energy passing through an additional filter to the deeper layer. Finally, wide-detector CT systems (Toshiba Medical Systems, Tustin, CA) can be used to acquire two spectrally distinct datasets with two consecutive 270° rotations around the same anatomic region at different peak potentials (80, 135 kVp) [5•].

Image Creation from DECT Data

Dual-energy images can be created using either an image-based or a projection-based approach. The projection-based approach requires both low-energy and high-energy data obtained from the same, or nearly the same, view angle. The projection-based approach is used for data acquired with rapid tube potential switching between projection views and switching between rotations, as well as for dual-layer detectors. The image-based approach must be used for datasets acquired with a dual-source scanner. The image-based approach is easier to implement because raw projection data are not required; however, this approach is more limited by beam hardening in both high-energy and low-energy images, which can result in artifacts in derived images [5•].

Mixed (i.e., combined, average-weighted) images (Fig. 1a) are created with variable contributions from low-energy and high-energy data reconstructed as two separate SECT image sets. A mixed image with 70 % contribution from 140-kVp images and 30 % from 100-kVp images yields images equivalent to conventional 120-kVp SECT images. Mixed images with a higher percentage of lower-energy data will have higher contrast but higher noise, whereas images with a higher percentage of higher-energy data will have lower image contrast and lower noise.

Virtual monochromatic images can be generated from dual-energy data to display tissue attenuation properties similar to those that would result from imaging with a monochromatic beam at a single energy level (Fig. 1b). With a projection-based approach, data are first postprocessed to minimize beam-hardening artifacts, and density projections of water and iodine are then used to reconstruct water-equivalent and iodine-equivalent density images. Monochromatic images are obtained from a linear combination of water and iodine images at the desired x-ray energy level [5•]. With the image-based approach, monochromatic images are created from a linear combination of low-energy and high-energy image sets with the weighting required to achieve the desired x-ray energy level [4].

Differentiation of tissues depends on differences in attenuation measured at two energy levels [1]. A basis material decomposition process is used to divide (decompose) unknown tissue within a voxel into selected materials (e.g., iodine and water) with known attenuation properties at high and low tube potentials. The identification of iodine using this method allows the generation of a blood-pool image displaying only iodine or a virtual noncontrast image displaying no iodine. Iodine maps can be depicted as gray-scale conventional images or superimposed as a color overlay on mixed images.

Cardiovascular Applications

Performing Myocardial Perfusion Imaging

Coronary CT angiography is well-established for evaluation of coronary artery stenosis, especially in patients with low to intermediate probability of coronary artery disease (CAD), because of its high negative predictive value (NPV) and sensitivity. However, its specificity is not high, especially in patients with intermediate grades of stenosis (30 – 80 %), as CT does not help determine which stenotic lesions are hemodynamically significant. In other words, coronary CT angiography alone is not effective in predicting myocardial ischemia. However, CT can provide physiological information (perfusion) and anatomic information (luminal stenosis), giving it a unique advantage over other techniques.

A stress-perfusion CT protocol typically has three phases: stress perfusion (adenosine/regadenoson); rest perfusion,

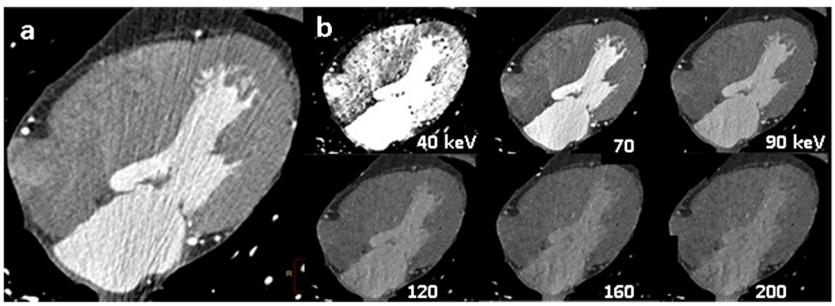

Fig. 1 Example images created from dual-energy data in a subject with normal cardiac morphology and function: **a** mixed image resembling single-energy image at 120 kVp; **b** virtual monochromatic images at selected energies from 40 to 200 keV

which includes coronary CT angiography after premedication with beta-blockers and sublingual nitroglycerin; and delayed (10 – 15 min) enhancement to evaluate for myocardial infarct and viability. Perfusion imaging can be performed either in a static mode (during the arterial phase of contrast enhancement) or in a dynamic mode (at different time points after contrast agent administration), the latter with an increased radiation dose but allowing quantification of perfusion. Ischemia is diagnosed when there is a defect under stress but not under rest perfusion; infarct is diagnosed when there is a defect under both stress and rest perfusion.

Although SECT is most commonly used for CT myocardial perfusion imaging, DECT offers the advantage of decreased beam hardening at the interface between the ventricular blood pool and endocardium; beam hardening can give rise to heterogeneous attenuation that may be confused with pathology. Several studies have demonstrated the utility of DECT in the evaluation of myocardial perfusion, particularly DECT-derived iodine maps representing the myocardial blood pool superimposed on a grayscale anatomic multiplanar reformat (MPR) of the myocardium in short-axis, long-axis, and four-chamber orientations, in comparison to MRI or SPECT.

Kang et al. found that DECT had 84 % sensitivity, 95 % specificity, and 92 % accuracy in detecting fixed perfusion defects on a per-segment basis, and 93 % sensitivity, 99 % specificity, and 97 % accuracy in detecting reversible defects compared with MRI [1]. Kim et al. found that DECT iodine maps had 77 % sensitivity, 94 % specificity, 53 % positive predictive value (PPV), and 98 % NPV for detecting myocardial perfusion defects compared with MRI, with a 5 % false-positive rate due to motion, beam hardening, image reconstruction errors, or malalignment [6]. In a study of patients with acute chest pain, Weininger et al. found that DECT (SPECT) had 93 % (94 %) sensitivity, 99 % (98 %) specificity, 92 % (88 %) PPV, and 96 % (94 %) NPV in detecting perfusion defects compared with perfusion MRI on a per-segment basis [7••]. These results are comparable to those seen with real-time dynamic perfusion SECT (versus SPECT), which demonstrated 86 % (84 %) sensitivity, 98 % (92 %) specificity, 94 % (88 %) PPV, and 96 % NPV (92 %) compared with perfusion MRI in the detection of perfusion defects [8••]. In a study of 47 patients, Arnoldi et al. found that DECT-based iodine maps are more effective in visual detection of perfusion defects than high-energy, low-energy, and mixed images when compared with SPECT, with 93 % sensitivity, 98 % NPV, and 88 % accuracy compared with SPECT in the detection of fixed perfusion defects, and 91 % sensitivity, 97 % NPV, and 93 % accuracy in the detection of mixed perfusion defects, and the highest area under the curve (AUC) values (0.84 – 0.93). However, single-energy and mixed images had higher specificity (84 – 98 %) for perfusion defects [9]. Meinel et al. found that DECT perfusion iodine maps had 99 % sensitivity and 97 % specificity in the detection of myocardial perfusion abnormalities compared with SPECT [8••]. However, of the reversible defects detected on SPECT, 45 % were misclassified by rest-stress CT as fixed defects.

Several studies have examined the potential of extracting both perfusion and luminal stenosis data from a single CT image set. Ruzsics et al. found that DECT iodine maps had 84 % sensitivity, 94 % specificity, and 92 % accuracy in the detection of ischemia compared with SPECT. CT angiography from the same DECT data demonstrated 98 % sensitivity, 88 % specificity, and 92 % accuracy in the detection of >50 % stenosis compared with coronary catheterization [10] (Fig. 2). In a subsequent study, DECT iodine maps were shown to have 92 % sensitivity, 93 % specificity, and 93 % accuracy in the detection of perfusion defects seen on SPECT, and 90 % sensitivity, 94 % specificity, and 93 % accuracy for the detection of >50 % stenosis seen on coronary angiography [11]. DECT iodine maps identified 96 % of fixed defects and 88 % of reversible defects, but DECT was not able to further differentiate between myocardial infarction and reversible ischemia in all patients [7••].

Several studies have shown that adding DECT perfusion data to SECT coronary CT angiography can reduce false-positive results, resulting in a higher accuracy than seen with SPECT alone and a higher specificity than seen with CT coronary angiography alone. Wang et al. found that DECT had 68 % sensitivity and 93 % specificity compared with SPECT in the detection of perfusion defects; the accuracy improved from 86 % for coronary CT angiography alone to 88 % for coronary CT angiography plus DECT perfusion, as compared with invasive coronary angiography [12]. In two studies, Ko et al. found that DECT iodine maps identified 89 % of reversible defects seen on MRI with 82 % specificity on a per-segment basis and 91 % sensitivity, 72 % specificity, and 83 % accuracy on a per-vessel basis compared with stress MRI [13] (Figs. 3 and 4). DECT iodine maps also had a sensitivity of 89 % and specificity of 76 % for identifying vascular territories with significant stenosis on coronary angiography. When DECT perfusion was added to coronary CT angiography, the per-vessel sensitivity increased from 92 % to 93 %, specificity increased from 68 % to 86 %, and PPV increased from 74 % to 88 % in comparison with coronary angiography alone [14]. Meyer et al. found that DECT had 90 % sensitivity and 71 % specificity in the detection of CAD compared with MRI [15].

Radiation dose is a concern with DECT myocardial perfusion imaging because of the requirement to acquire multiple phases. However, even with rest DECT, 88 % of reversible perfusion defects seen on SPECT can be detected with DECT iodine maps [16]. Rest CT perfusion imaging has also been found to display an enhancement pattern due to diminished capacitance of microvessels in the subendocardium during systole in patients with ischemia [17]. Meinel et al. found that delayed DECT can be omitted in a stress protocol without

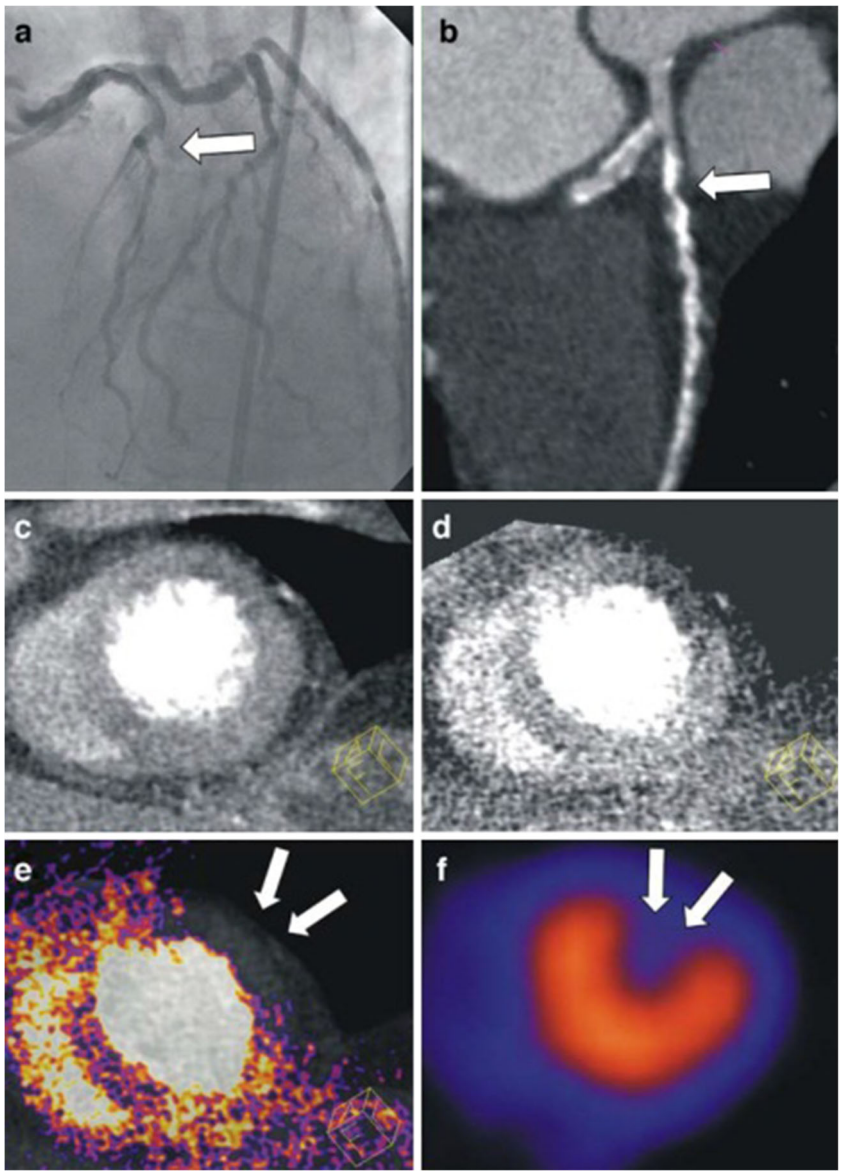

Fig. 2 Contrast-enhanced retrospectively ECG-gated helical DECT study in a 74-year-old woman with abnormal SPECT. **a**, **b** Coronary angiogram (**a**) and corresponding coronary CT angiography reconstruction image based on mixed energy spectra (**b**) show subtotal occlusion (*arrows*) of the first diagonal branch (D1) by predominantly calcified atherosclerotic plaque. **c**, **d** The myocardial iodine content is analyzed based on 140 kVp (**c**) and 80 kVp (**d**) x-ray spectra reconstructions. **e**, **f** The color-coded "iodine map" representing the myocardial blood pool is superimposed onto virtually nonenhanced short-axis reformats (**e**) and delineates a blood pool deficit (*arrows*) in the anterolateral myocardial D1 territory in good correlation with the fixed perfusion defect seen on the SPECT image (**f**). With kind permission from Springer Science+ Business [10]

losing accuracy: rest-only DECT showed 92 % sensitivity and 98 % specificity, whereas stress-only, rest-stress, stress and delayed DECT, and a combination of all three demonstrated 99 % sensitivity and 97 % specificity; there was no increased accuracy with the addition of a delayed DECT phase [14]. Mean effective radiation doses for rest, stress, and delayed DECT were 5.6, 7.1, and 4.6 mSv, respectively.

Myocardial perfusion quantification requires dynamic imaging, which largely has not been explored with DECT. Beam hardening can interfere with myocardial perfusion quantification due to distortion of arterial and myocardial time–density curves used to estimate perfusion. DECT-generated images, particularly monochromatic images at a higher energy (keV), offer the potential to reduce beam-hardening artifacts, thereby improving the accuracy of myocardial perfusion quantification compared to SECT.

A dynamic scan performed in a porcine model using rapid tube potential switching DECT demonstrated accurate iodine time–density curves and myocardial perfusion with virtual monochromatic 70-keV images [3]. In a myocardial phantom model scanned using the same technique, 70-keV images derived using a projection-based approach provided more uniform enhancement throughout normal myocardium during the first pass, with consistent time-delay curves from different parts of the myocardium, in comparison to SECT and image-based DECT. This method also achieved the highest contrast-to-noise ratio (CNR), reduced beam hardening, and improved myocardial perfusion quantification [3]. Decreases in beam hardening with virtual monochromatic 69-keV images obtained again with rapid tube potential switching have also been demonstrated in ex vivo imaging of human hearts [18].

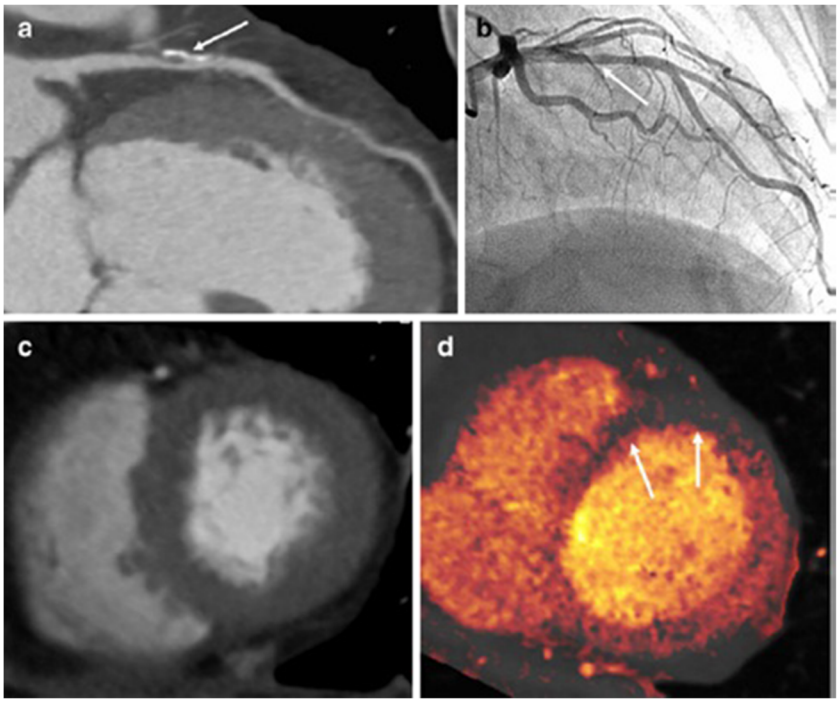

Fig. 3 Images from a 66-year-old man with dyspnea and chest pain. **a** Coronary CT angiogram shows moderate stenosis with mixed calcified and noncalcified plaque in the proximal segment of the left anterior descending (LAD) coronary artery (*arrow*). **b** Conventional coronary angiogram does not reveal significant stenosis in the corresponding segment of the LAD artery (*arrow*). **c** The rest CT perfusion dual-source CT image does not show any perfusion defects in the left ventricular (LV) myocardium. **d** The dual-energy CT-based iodine map during adenosine infusion reveals a perfusion defect in the apical anterior and anteroseptal LV myocardium (*arrows*). The false-positive finding in the apical anterior and anteroseptal wall is related to the beam hardening artifact. With kind permission from Springer Science+Business [13]

The physiological significance of coronary stenosis can also be assessed by evaluating coronary artery flow during the DECT stress phase; a coronary enhancement ratio (CER) can be calculated by dividing mean attenuation in the proximal and distal portions of a coronary artery by attenuation in the aortic root. In one study, the CER determined from dual-source DECT was found to be lower in ischemic territories detected by stress perfusion imaging and in stenosed coronary arteries identified by coronary CT angiography [19]. This approach had a sensitivity of 86 % and specificity of 75 % for separating ischemic and nonischemic territories compared to stress perfusion imaging. CER decreased with the progression of coronary stenosis as determined from coronary angiography. Lower CER (<0.8) correlated negatively with the physiological significance of CAD [16].

Assessing Myocardial Infarction and Viability

In patients with established myocardial infarction, MRI or positron emission tomography is often used to assess for the presence of viable myocardium and determine suitability for revascularization procedures. Delayed-enhancement MRI is performed to identify infarct and nonischemic causes of cardiac failure. CT is an alternative imaging modality that may be used to diagnose myocardial infarction. Myocardial infarcts present as hypoattenuating tissue on rest scans (either standard or perfusion scans). Alternatively, infarcts may enhance on delayed scans.

Arterial Phase Imaging

Infarcts are more conspicuous on DECT-generated iodine maps or low-keV monochromatic images than on polychromatic images. In a canine infarct model with histopathology as the gold standard, Peng et al. found that evaluation of DECT myocardial iodine maps in addition to SECT from a dual-source scanner were comparable to rest SPECT myocardial perfusion imaging for detection of acute myocardial infarction and superior to SECT alone [20]: the sensitivity, specificity, PPV, NPV, and accuracy were 88 %, 93 %, 81 %, 93 %, and 93 %, respectively, for SECT plus iodine maps, and 83 %, 90 %, 75 %, 94 %, and 88 % for SPECT. CT values of infarcted myocardium were significantly lower than those of noninfarcted myocardium on 80-kVp, 140-kVp, and average-weighted 120-kVp images [19].

In a porcine infarct model, arterial phase DECT iodine maps from a dual-source scanner were more effective than a 100-kVp images, showing 72 % sensitivity and 88 % specificity compared with 78 % sensitivity and 92 % specificity for

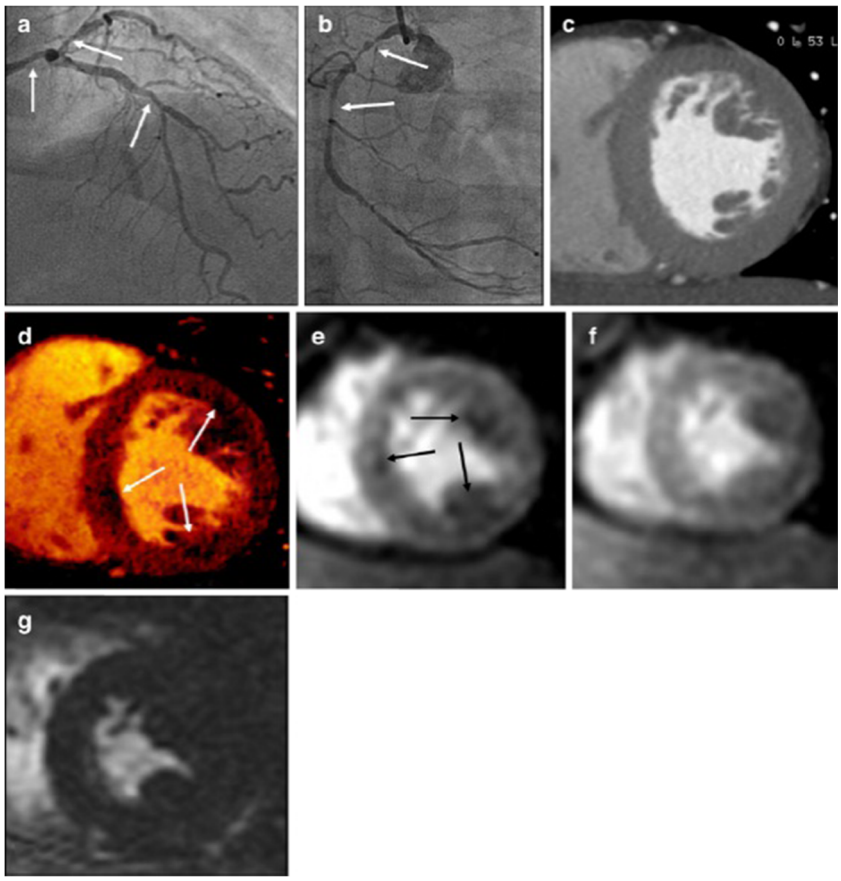

Fig. 4 Images from a 55-year-old woman with angina. **a**, **b** Conventional coronary angiograms show significant stenosis (*arrows*) in the left main mid-segment of the left anterior descending and the proximal segment of the left circumflex coronary arteries (**a**) and the proximal segment of the right coronary artery (**b**). **c** The CT perfusion image at rest does not show any perfusion defects in the left ventricular (LV) myocardium. **d** The dual-energy CT-based iodine map during adenosine infusion reveals a concentric perfusion defect in the mid-LV myocardium. **e**, **f** The findings in **d** are in good correlation with cardiac MRI findings acquired at rest (**e**) and stress (**f**), which reveal reversible subendocardial perfusion defects in the same myocardial areas. **g** Delayed enhanced cardiac MRI image does not show any delayed enhancement along the mid-LV myocardium. With kind permission from Springer Science+Business [13]

delayed-enhancement MRI, with histopathology as the gold standard [21].

Similar results have been seen in clinical studies. In one study, hypoattenuation on iodine maps from rest perfusion DECT data had 90 % sensitivity for the detection of infarct seen on SPECT [7••, 9]. In patients undergoing CT angiography for coronary bypass graft patency, Bauer et al. found that mixed images from arterial phase DECT demonstrated the best results overall, with 77 % sensitivity, 97 % specificity, 85 % PPV, 96 % PPV, and 94 % accuracy for the detection of myocardial infarct compared to 3-T cardiac MRI [22]. However, 100-kVp grayscale images had the highest sensitivity (80 %) for the detection of myocardial scar; iodine maps were prone to artifacts, especially from sternal wires, which reduced sensitivity to 70 % [21].

Delayed Phase Imaging

Enhancement on CT images acquired 10 to 15 min after injection of contrast medium, either in a subendocardial or transmural pattern in a vascular distribution, is also an indicator of myocardial infarction. Iodine-based contrast medium accumulates in the expanded extracellular space of the myocardium (myocardial infarct) or fibrosis (cardiomyopathy). Although CT can be used for delayed imaging, it has a lower signal-to-noise ratio and CNR than MRI, making it less sensitive. DECT iodine maps offer improved conspicuity of delayed enhancement compared to SECT.

In a porcine infarct model, late-enhancement DECT using iodine maps superimposed on grayscale MPRs had per-segment sensitivities of 77 % to 92 % compared to histopathology; 100-kVp images had 62 % to 97 % sensitivity, and delayed-enhancement MRI had 79 % to 94 % sensitivity. There was no significant difference in diagnostic accuracy among late-enhancement DECT, 100-kVp late-enhancement DECT, and MRI (90 %, 89 %, and 90 %, respectively) [23]. A study in patients with CAD demonstrated 82 % sensitivity, 98 % specificity, 95 % NPV, 89 % PPV, and 95 % accuracy for detecting infarcts with delayed-enhancement DECT compared with delayed enhancement MRI [1]. There was a close, linear correlation between MRI and late-enhancement DECT for the percentage of infarct area on a per-section basis.

Characterizing Coronary Artery Plaque

Coronary artery calcium quantification is used in risk stratification for cardiovascular disease, and improves the accuracy of current multivariate risk factor models. Noncontrast CT is

typically performed to quantify coronary calcium, whereas contrast-enhanced CT is performed to evaluate coronary arterial luminal stenosis. The estimation of calcium burden from coronary CT angiograms is sometimes desired but is limited by extensive overlap of attenuation values for calcium and iodine.

DECT has demonstrated the potential for separating calcium from contrast-enhanced lumen. Material decomposition has been used to generate virtual noncontrast images suitable for calcium scoring from arterial phase DECT data. One study using dual-source DECT showed an excellent correlation between calcium volumes quantified from virtual and true noncontrast images on a per-patient and per-vessel basis, although the overall calcium volumes from virtual noncontrast images were lower [24]. It is unclear whether the lower volume of calcium on virtual noncontrast images was a more accurate measure of calcium because of less beam hardening and blooming artifact or if the lower volume was less accurate because of removal of iodine and calcium during the generation of the virtual noncontrast images. Another study using fast-switching tube potential DECT demonstrated a good correlation between virtual noncontrast-derived and true noncontrast-derived Agatson, mass, and volume calcium scores, both in phantoms and in patients [25]. Boll et al. also found improved coronary plaque quantification with contrast-enhanced images obtained with dual layer detectors: calcified plaque size was overestimated in low-energy images and underestimated in high-energy images, but was accurately estimated using combined images, with optical coherence tomography as the gold standard [26].

Of greater interest than identifying coronary calcium is identifying noncalcified coronary plaques, as identification of these plaques is essential for initiation of treatment to prevent plaque rupture, the cause of acute coronary events. Although attempts have been made to classify plaques based on attenuation measurements with SECT, this has largely only been successful in distinguishing between calcified and noncalcified plaques only, not in distinguishing among noncalcified plaque components, because of significant overlap in attenuation values [27].

Although combined attenuation data from DECT has greater potential for plaque characterization than SECT, results from initial DECT studies have not been encouraging. Barreto et al. [28] scanned excised human coronary arteries consecutively at 80 and 140 kVp and identified plaques based on histology. There was higher attenuation of densely calcified and fibrocalcified plaques, but not fibrous and lipid-rich plaques, at 80 kVp. Tanami et al., in another ex vivo study, scanned human coronary arteries at 80, 100, 120, and 140 kVp and correlated the results with histology. Again, the attenuation of lipid-rich and fibrous plaques at all energy levels overlapped. However, the AUC for differentiating lipid-rich plaques from fibrotic core was higher at 80 and 100 kVp than at 120 or 140 kVp. In addition, the AUC for the ratio of attenuation at 80 and 140 kVp was better than the AUC for attenuation at any single energy. Hence, performance was improved at lower tube potentials and by combining high-attenuation and low-attenuation data [29]. However, Henzler et al. [30] performed dual-source DECT and SECT in excised hearts with histopathology as the gold standard and found no significant differences in mean attenuation values among the various plaque types with the different scan techniques. These studies suggest that differences among noncalcified coronary plaques may not be large enough to produce significantly distinct attenuation values within the diagnostic energy range.

Assessing Coronary Stents

Patients with coronary artery stents may experience in-stent restenosis or complications related to the stents. Stent evaluation is challenging on CT because of overlap in the attenuation values of stent struts and iodinated blood as well as artifacts. Partial volume averaging causes the metal stent and any areas of calcium to appear larger than they are in reality, resulting in an artificially smaller lumen. Additionally, beam hardening distorts the CT density adjacent to the stent–lumen interface. Luminal narrowing from these artifacts can be as much as 62 % to 94 % [31]. Studies to date have provided mixed results regarding DECT's potential to improve stent assessment.

Boll et al. found that DECT using dual-layer detectors enabled evaluation of the stent lumen and mesh beyond what is achievable with SECT [32]. Four stents ranging in size from 2 to 5 mm filled with contrast medium were evaluated longitudinally and axially in a moving anthropomorphic heart phantom. Data were postprocessed using an enhancement algorithm based on high-energy and low-energy absorption profiles. Stent lumen depiction and stent mesh delineation were quantified in terms of CNR and kurtosis, respectively. For smaller stents, CNR and kurtosis were higher for imaging in the axial plane with a lower peak potential and with application of the enhancement algorithm to 80-kVp data. Lower energies increased attenuation of the contrast medium, which improved luminal depiction, but at the expense of higher noise. For larger stents, CNR and kurtosis were higher when stents were imaged at higher potentials in the longitudinal plane and with the enhancement algorithm applied to 140-kVp data. Higher energies are required for larger stents to overcome blooming artifacts and noise associated with more stent mesh material.

Halpern et al. found that stents could not be easily distinguished from iodinated contrast medium using a dual-layer detector [31]. Stents of various sizes were filled with iodinated contrast medium and submerged in water. Stent lumens were underestimated by 50 % on combined-energy images (equivalent to clinical CT images). A 24 % decrease in strut

thickness and 25 % increase in stent luminal diameter were demonstrated on high-energy images relative to low-energy images based on observer measurements. However, with full-width half-maximum measurements based on automatic edge detection, no significant changes in stent luminal diameter or strut thickness were detected, suggesting no true improvement at higher tube potentials.

Higher-keV monoenergetic images generated from DECT data may improve evaluation of stents by reducing beam-hardening artifacts [33]. A patient study by Secchi et al. demonstrated a significant decrease in the diameter of artifacts arising from coronary stents at a higher energy (5.9 mm at 40 keV, 2.7 mm at 120 keV) [34].

Detecting and Quantifying Myocardial Iron Deposition

Detection of myocardial iron is essential in patients who have cardiac iron overload caused by transfusion therapy, so that early chelation can be initiated and cardiac failure avoided. This assessment is typically performed with MRI, using a multiecho T2-weighted gradient echo sequence to calculate myocardial T2*. A T2* value <20 ms is associated with cardiac failure. DECT offers the potential to identify and quantify myocardial iron and may provide an alternative to MRI.

Imaging of agarose phantoms at various iron concentrations with DECT using two sources (80 or 100/140 kVp) demonstrated a strong correlation between iron content and attenuation and between iron content and attenuation differences at different energy levels and a moderate correlation between iron content and attenuation ratios (except 80/140 kVp) using MRI as the reference standard [35]. In another study, Hazirolan et al. performed DECT over a 30-mm range at the mid-level of the heart using two sources in 19 patients with thalassemia [36]. Attenuation values of the septum and paraspinal musculature were measured on 80-kVp, 140-kVp and weighted-average (30 %, 80 kVp; 70 %, 140 kVp) images and correlated with T2* MR images. T2* values had a significant negative correlation with attenuation of septal muscle, strong for 80-kVp and weighted-average images and good for 140-kVp images, but no correlation with attenuation of paraspinal muscle. The mean DECT dose was 0.71 mSv.

Evaluating Aortic Disease

CT is routinely used for the evaluation of aortic disease. Noncontrast scans, in addition to arterial and venous scans, are sometimes required. For example, a noncontrast scan is performed in patients with suspected acute aortic syndrome for the evaluation of intramural hematoma or intimal calcification. In patients evaluated for follow-up of aortic endovascular stent grafts, a noncontrast phase is required for evaluation of calcifications, which may be confused with endoleaks on postcontrast scans [37]. DECT data obtained during the arterial or venous phase can be used to generate virtual noncontrast images, obviating the need for a noncontrast scan and thus minimizing the radiation dose [38–42] (Fig. 5).

In a study of 30 patients after endovascular stent graft repair, Numburi et al. compared arterial DECT using two tubes (80/140 kVp) and venous SECT (120 kVp) with a standard triple-phase protocol obtained at different time points in the same patient [38]. Tissue attenuation characteristics were similar on virtual and true noncontrast scans except for stent struts and calcium; decreased stent and calcium attenuation was noted on some virtual noncontrast scans as a result of overlap between their attenuation values and the attenuation values of iodine. An additional limitation of virtual noncontrast scans noted in this and other studies [43] was the presence of pulsation artifacts visible because of insufficient iodine removal. Still, virtual and true noncontrast images were shown to provide equivalent diagnostic information, suggesting that a SECT noncontrast and SECT arterial phase acquisition could be replaced with a DECT arterial phase acquisition, achieving a 31 % reduction in radiation dose [38].

Chandarana et al. found that mean radiation dose was reduced by 60 % (28 to 11 mSv) using only virtual noncontrast images generated from dual-source DECT imaging during the venous phase to evaluate possible endoleaks; this technique achieved high sensitivity for endoleak detection compared with a triple-phase criterion standard [39]. Stolzmann et al. achieved similar results with only delayed-phase dual-source DECT imaging, with an accuracy, sensitivity, specificity, NPV, and PPV of 96 % to 100 % for endoleak detection compared to triple-phase studies [41]. Similar results have been shown for DECT with rapid tube potential switching technology. In a study of 78 patients with endovascular stent grafts, the sensitivity (reader 1/reader 2) for endoleak detection with virtual noncontrast images created from DECT arterial phase data was 83 %/75 % and with virtual noncontrast images generated from DECT venous phase data was 96 %/88 %, suggesting that a 40 % dose reduction could be achieved by eliminating a true noncontrast phase or a 64 % dose reduction could be achieved by eliminating both a noncontrast and arterial phase imaging [42]. Maturen et al. also demonstrated that sensitivity for endoleak detection and overall endoleak conspicuity rankings were higher on monoenergetic 55-keV images than on 75-keV images (equivalent to 120 kVp images) generated from DECT data obtained using rapid tube potential switching [44], suggesting routine reconstruction of lower-energy monochromatic images for endoleak surveillance.

Radiation Dose Requirements

For dual-source technology, several studies have shown no increase in radiation with dual-energy compared to single-

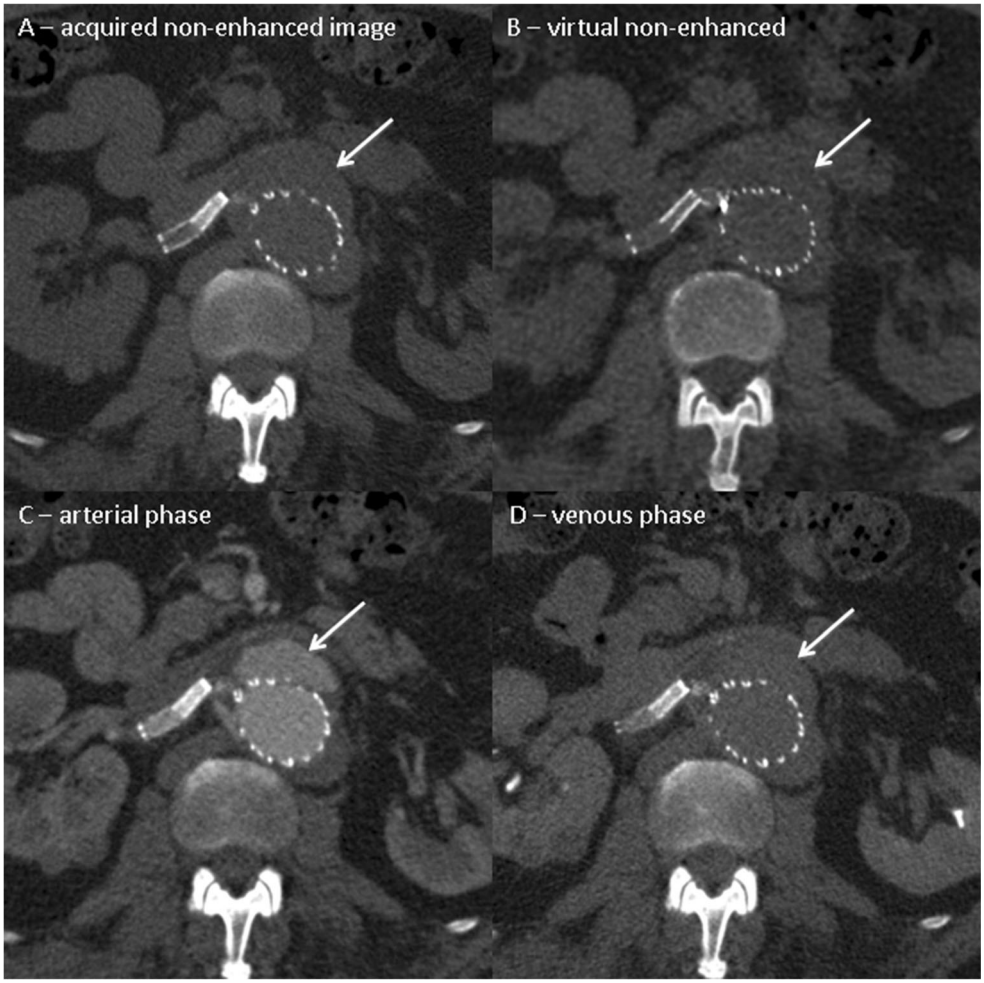

Fig. 5 Example of an endoleak (*arrow*) in a patient with abdominal aortic aneurysm treated with an endovascular stent graft with a side stent to the right renal artery. Shown are the three acquired image phases (**a** nonenhanced phase, **b** arterial phase, **c** venous phase) and **d** the virtual nonenhanced phase

energy scans. In a phantom study, Schenzle et al. demonstrated similar radiation doses for 80/140 kVp on a first-generation dual-source system (2.6 mSv), 100/140 kVp on a second-generation dual-source system (2.7 mSv), and 120 kVp SECT on a dual-source CT system (2.7 mSv) at comparable noise levels [45]. A patient study showed a lower dose with DECT coronary angiography (4.5±1.9 mSv) than with SECT (9.8± 4.8 mSv), with higher CNR and comparable diagnostic image quality [46].

DECT on a dual-source scanner has also been shown to reduce radiation dose by replacing a SECT arterial or venous phase scan and eliminating one or more phases of a triple contrast phase study in patients evaluated after endovascular stent graft repair [40–42]. Similarly, the dose for myocardial perfusion CT can be reduced by limiting evaluation to DECT data acquired during stress and rest phases only [15].

Only limited, inconclusive information is available regarding radiation dose requirements for DECT with rapid tube potential switching technology [47]. As with dual-source CT, DECT with tube potential switching has demonstrated dose reduction through elimination of one phase of a triple contrast phase study [41]. Radiation dose requirements for DECT with dual-layer detectors are not yet established. With dual-layer detectors, DECT data are acquired at 140 kVp, which represents an increase in tube potential in most cardiovascular patients. It may be possible, in practice, to compensate for the increase in tube potential by reducing the tube current, but further study of this practice is needed. As with other approaches to DECT, the potential exists to eliminate one or more phases of a multiphase study using dual-layer technology.

Contrast Dose Requirements

The inclusion of lower-energy data in a DECT-based image can permit the use of less iodinated contrast medium because the attenuation of iodine is higher at lower x-ray energies (iodine attenuation is approximately 70 % higher for CT imaging at a peak tube potential of 80 kVp than at 140 kVp). The inclusion of low-energy data leads to higher CNR of coronary arteries when the contrast medium dose is held constant [45]. This supports the idea that DECT may be

used to decrease the amount of contrast medium used in the evaluation of coronary arteries.

Conclusions

DECT is useful in several cardiovascular indications without a radiation dose penalty. DECT images improve the conspicuity of myocardial perfusion defects, which enables identification of hemodynamically significant coronary lesions. This technique also improves detection of scar on delayed-enhancement images. DECT data acquired from coronary arteries during an arterial phase can be used to create virtual noncontrast images useful for quantifying coronary calcium. DECT has some potential for coronary plaque characterization, particularly in distinguishing between calcified and noncalcified components. Artifacts from stents can be decreased by using higher-energy monochromatic images. DECT arterial or venous phase data can be used to create virtual noncontrast images and reduce overall radiation dose by eliminating acquisition of noncontrast data for evaluation of the aorta. The value of DECT is gradually being established for specific cardiovascular CT indications and its use is expected to increase as dual-energy capable CT scanners become more widely available.

Acknowledgements We are grateful for the editorial assistance of Megan M. Griffiths, scientific writer for the Imaging Institute, Cleveland Clinic, Cleveland, Ohio.

Compliance with Ethics Guidelines

Conflict of Interest Prabhakar Rajiah and Sandra Hallburton declare that they have no conflict of interest.

Human and Animal Rights and Informed Consent This article does not contain any studies with human or animal subjects performed by any of the authors.

References

Papers of particular interest, published recently, have been highlighted as:
- • Of importance
- •• Of major importance

1. Kang DK, Schoepf UJ, Bastarrika G, Nance Jr JW, Abro JA, Ruzsics B. Dual-energy computed tomography for integrative imaging of coronary artery disease: principles and clinical applications. Semin Ultrasound CT MR. 2010;31:276–91.
2. Flohr TG, McCollough CH, Bruder H, et al. First performance evaluation of a dual-source CT (DSCT) system [erratum in Eur Radiol. 2006;16:1405]. Eur Radiol. 2006;16:256–68.
3. So A, Lee TY, Imal Y, et al. Quantitative myocardial perfusion imaging using rapid kVp switch dual energy CT: a preliminary experience. J Cardiovasc Comput Tomogr. 2011;5(6):430–2.
4. Roessl E, Herrmann C, Kraft E, Proksa R. A comparative study of a dual-energy-like imaging technique based on counting-integrating readout. Med Phys. 2011;38:6416–28.
5.• So A, Hsieh J, Narayanan S, et al. Dual-energy CT and its potential use for quantitative myocardial CT perfusion. J Cardiovasc Comput Tomogr. 2012;6:308–17. *The authors describe the use of rapid tube potential switching technology for quantitative myocardial perfusion CT. This method of data acquisition permits creation of virtual monochromatic images using a projection-based approach with significantly decreased beam-hardening artifacts compared to standard CT images. The reduction of beam-hardening artifacts is important because these artifacts can induce non-uniform shifts in CT numbers and confound assessment of myocardial perfusion.*
6. Kim SM, Chang SA, Shin W, Choe YH. Dual-energy CT perfusion during pharmacologic stress for the assessment of myocardial perfusion defects using a second-generation dual-source CT: a comparison with cardiac magnetic resonance imaging. J Comput Assist Tomogr. 2014;38:44–52.
7.•• Weininger M, Schoepf UJ, Ramachandra A, et al. Adenosine-stress dynamic real-time myocardial perfusion CT and adenosine-stress first-pass dual-energy myocardial perfusion CT for the assessment of acute chest pain: initial results. Eur J Radiol. 2012;81:3703–10. *The authors describe initial experience in performing myocardial stress perfusion CT in a clinical population with acute chest pain and demonstrated that compared to both SPECT and MRI, dynamic real-time perfusion CT and first-pass dual-energy perfusion CT show good agreement for detection of myocardial perfusion defects.*
8.•• Meinel FG, De Cecco CN, Schoepf UJ, et al. First-arterial-pass dual-energy CT for assessment of myocardial blood supply: do we need rest, stress, and delayed acquisition? Comparison with SPECT. Radiology. 2014;270:708–16. *This comparison study with SPECT shows that the accuracy of DECT for assessment of the myocardial blood supply is not increased by the addition of a delayed DECT acquisition and concludes that the delayed scan may be omitted to reduce radiation exposure. The authors also demonstrate that almost 50 % of defects defined as reversible with SPECT were misclassified as fixed with rest–stress DECT and warn clinicians interpreting DECT myocardial perfusion studies about this discrepancy.*
9. Arnoldi E, Lee YS, Ruzsics B, et al. CT detection of myocardial blood volume deficits: dual-energy CT compared with single-energy CT spectra. J Cardiovasc Comput Tomogr. 2011;5:421.
10. Ruzsics B, Lee H, Zwerner PL, Gebregziabher M, Costello P, Schoepf UJ. Dual-energy CT of the heart for diagnosing coronary artery stenosis and myocardial ischemia – initial experience. Eur Radiol. 2008;18:2414–24.
11. Ruzsics B, Schwarz F, Schoepf UJ, et al. Comparison of dual-energy computed tomography of the heart with single photon emission computed tomography for assessment of coronary artery stenosis and of the myocardial blood supply. Am J Cardiol. 2009;104:318–26.
12. Wang R, Yu W, Wang Y, et al. Incremental value of dual-energy CT to coronary angiography for the detection of significant coronary stenosis: comparison with quantitative coronary angiography and single photon emission computed tomography. Int J Cardiovasc Imaging. 2011;27:647–56.
13. Ko SM, Choi JW, Song MG, et al. Myocardial perfusion imaging using adenosine-induced stress dual-energy computed tomography of the heart: comparison with cardiac magnetic resonance imaging and conventional coronary angiography. Eur Radiol. 2011;21:26–35.
14. Ko SM, Choi JW, Hwang HK, Song MG, Shin JK, Chee HK. Diagnostic performance of combined noninvasive anatomic and

functional assessment with dual-source CT and adenosine-induced stress dual-energy CT for detection of significant coronary stenosis. AJR Am J Roentgenol. 2012;198:512–20.
15. Meyer M, Nance Jr JW, Schoepf UJ, et al. Cost-effectiveness of substituting dual-energy CT for SPECT in the assessment of myocardial perfusion for the workup of coronary artery disease. Eur J Radiol. 2012;81:3719–25.
16. Heymann MA, Payne BD, Hoffman JI, Rudolph AM. Blood flow measurements with radionuclide-labeled particles. Prog Cardiovasc Dis. 1977;20:55–79.
17. Nagao M, Matusjoka H, Kawakami H, et al. Quantification of myocardial perfusion by contrast-enhanced 64-MDCT: characterization of ischemic myocardium. AJR Am J Roentgenol. 2008;191: 19–25.
18. Yamada M, Jinzaki M, Kuribayashi S, Imanishi N, Funato K, Aiso S. Beam-hardening correction for virtual monochromatic imaging of myocardial perfusion via fast-switching dual-kVp 64-slice computed tomography: a pilot study using a human heart specimen. Circ J. 2012;76:1799–801.
19. Nagao M, Kido T, Watanabe K, et al. Functional assessment of coronary artery flow using adenosine stress dual-energy CT: a preliminary study. Int J Cardiovasc Imaging. 2011;27:471–81.
20. Peng J, Zhang LJ, Schoepf UJ, et al. Acute myocardial infarct detection with dual energy CT: correlation with single photon emission computed tomography myocardial scintigraphy in a canine model. Acta Radiol. 2013;54:259–66.
21. Kerl JM, Deseive S, Tandi C, et al. Dual energy CT for the assessment of reperfused chronic infarction: a feasibility study in a porcine model. Acta Radiol. 2011;52:834–9.
22. Bauer RW, Kerl JM, Fischer N, et al. Dual-energy CT for the assessment of chronic myocardial infarction in patients with chronic coronary artery disease: comparison with 3T MRI. AJR Am J Roentgenol. 2010;195:639–46.
23. Deseive S, Bauer RW, Lehmann R, et al. Dual-energy computed tomography for the detection of late enhancement in reperfused chronic infarction: a comparison to magnetic resonance imaging and histopathology in a porcine model. Invest Radiol. 2011;46: 450–6.
24. Schwarz F, Nance Jr JW, Ruzsics B, Bastarrika G, Sterzik A, Schoepf UJ. Quantification of coronary artery calcium on the basis of dual-energy coronary CT angiography. Radiology. 2012;264: 700–7.
25. Yamak D, Pavlicek W, Boltz T, Panse PM, Akay M. Coronary calcium quantification using contrast-enhanced dual-energy computed tomographic scans. J Appl Clin Med Phys. 2013;14:4014.
26. Boll DT, Merkle EM, Paulson EK, Mirza RA, Fleiter TR. Calcified vascular plaque specimens: assessment with cardiac dual-energy multi detector CT in anthropomorphically moving heart phantom. Radiology. 2008;249:119–26.
27. Pohle K, Achenbach S, Macneill B, et al. Characterization of non-calcified coronary atherosclerotic plaque by multi-detector row CT: comparison to IVUS. Atherosclerosis. 2007;190:174–80.
28. Barreto M, Schoenhagen P, Nair A, et al. Potential of dual-energy computed tomography to characterize atherosclerotic plaque: ex vivo assessment of human coronary arteries in comparison to histology. J Cardiovasc Comput Tomogr. 2008;2:234–42.
29. Tanami Y, Ikeda E, Jinzaki M, et al. Computed tomographic attenuation value of coronary atherosclerotic plaques with different tube voltage: an ex vivo study. J Comput Assist Tomogr. 2010;34:58–63.
30. Henzler T, Porubsky S, Kayed H, et al. Attenuation-based characterization of coronary atherosclerotic plaque: comparison of dual source and dual energy CT with single-source CT and histopathology. Eur J Radiol. 2011;80:54–9.
31. Halpern EJ, Halpern DJ, Yanof JH, et al. Is coronary stent assessment improved with spectral analysis of dual energy CT? Acad Radiol. 2009;16:1241–50.
32. Boll DT, Merkle EM, Paulson EK, Fleiter TR. Coronary stent patency: dual-energy multidetector CT assessment in a pilot study with anthropomorphic phantom. Radiology. 2008;247:687–95.
33. Bamberg F, Dierks A, Nikolaou K, Reiser MF, Becker CR, Johnson TR. Metal artifact reduction by dual energy computed tomography using monoenergetic extrapolation. Eur Radiol. 2011;21:1424–9.
34. Secchi F, De Cecco CN, Spearman JV, et al. Monoenergetic extrapolation of cardiac dual energy CT for artifact reduction. Acta Radiol. 2014. doi:10.1177/0284185114527867.
35. Ibrahim EH, Bowman AW. Evaluation of iron overload: dual-energy computed tomography versus magnetic resonance imaging. J Cardiovasc Magn Reson. 2014;16:O92.
36. Hazirolan T, Akpinar B, Unal S, Gumruk F, Haliloglu M, Alibek S. Value of dual energy computed tomography for detection of myocardial iron deposition in thalassaemia patients: initial experience. Eur J Radiol. 2008;68:442–5.
37. Rozenblit AM, Patlas M, Rosenbaum AT, et al. Detection of endoleaks after endovascular repair of abdominal aortic aneurysm: value of unenhanced and delayed helical CT acquisitions. Radiology. 2003;227:426–33.
38. Numburi UD, Schoenhagen P, Flamm SD, et al. Feasibility of dual-energy CT in the arterial phase: imaging after endovascular aortic repair. AJR Am J Roentgenol. 2010;195:486–93.
39. Chandarana H, Godoy MC, Vlahos I, et al. Abdominal aorta: evaluation with dual-source dual-energy multidetector CT after endovascular repair of aneurysms – initial observations. Radiology. 2008;249:692–700.
40. Sommer WH, Graser A, Becker CR, et al. Image quality of virtual noncontrast images derived from dual-energy CT angiography after endovascular aneurysm repair. J Vasc Interv Radiol. 2010;21:315–21.
41. Stolzmann P, Frauenfelder T, Pfammatter T, et al. Endoleaks after endovascular abdominal aortic aneurysm repair: detection with dual-energy dual-source CT. Radiology. 2008;249:682–91.
42. Maturen KE, Kleaveland PA, Kaza RK, et al. Aortic endograft surveillance: use of fast-switch kVp dual-energy computed tomography with virtual noncontrast imaging. J Comput Assist Tomogr. 2011;35:742–6.
43. Shaida N, Bowden DJ, Barrett T, et al. Acceptability of virtual unenhanced CT of the aorta as a replacement for the conventional unenhanced phase. Clin Radiol. 2012;67:461–7.
44. Maturen KE, Kaza RK, Liu PS, Quint LE, Khalatbari SH, Platt JF. "Sweet spot" for endoleak detection: optimizing contrast to noise using low keV reconstructions from fast-switch kVp dual-energy CT. J Comput Assist Tomogr. 2012;36:83–7.
45. Schenzle JC, Sommer WH, Neumaier K, et al. Dual energy CT of the chest: how about the dose? Invest Radiol. 2010;45:347–53.
46. Kerl JM, Bauer RW, Maurer TB, et al. Dose levels of coronary CT angiography – a comparison of dual energy-, dual source-, and 16-slice CT. Eur Radiol. 2011;21:530–7.
47. Henzler T, Fink C, Schoenberg SO, Schoepf UJ. Dual-energy CT: radiation dose aspects. AJR Am J Roentgenol. 2012;199:S16–25.